Characterization of an RNA Granule from Developing Brain*[S]

George Elvira‡, Sylwia Wasiak§¶, Vanessa Blandford§, Xin-Kang Tong§, Alexandre Serrano‖, Xiaotang Fan§, Maria del Rayo Sánchez-Carbente‡, Florence Servant**, Alexander W. Bell**, Daniel Boismenu**, Jean-Claude Lacaille‖‡‡§§, Peter S. McPherson§¶¶, Luc DesGroseillers‡ ‡‡, and Wayne S. Sossin§‡‡‖‖‖

In brain, mRNAs are transported from the cell body to the processes, allowing for local protein translation at sites distant from the nucleus. Using subcellular fractionation, we isolated a fraction from rat embryonic day 18 brains enriched for structures that resemble amorphous collections of ribosomes. This fraction was enriched for the mRNA encoding β-actin, an mRNA that is transported in dendrites and axons of developing neurons. Abundant protein components of this fraction, determined by tandem mass spectrometry, include ribosomal proteins, RNA-binding proteins, microtubule-associated proteins (including the motor protein dynein), and several proteins described only as potential open reading frames. The conjunction of RNA-binding proteins, transported mRNA, ribosomal machinery, and transporting motor proteins defines these structures as RNA granules. Expression of a subset of the identified proteins in cultured hippocampal neurons confirmed that proteins identified in the proteomics were present in neurites associated with ribosomes and mRNAs. Moreover many of the expressed proteins co-localized together. Time lapse video microscopy indicated that complexes containing one of these proteins, the DEAD box 3 helicase, migrated in dendrites of hippocampal neurons at the same speed as that reported for RNA granules. Although the speed of the granules was unchanged by activity or the neurotrophin brain-derived neurotrophic factor, brain-derived neurotrophic factor, but not activity, increased the proportion of moving granules. These studies define the isolation and composition of RNA granules expressed in developing brain. ***Molecular & Cellular Proteomics 5:635–651, 2006.***

Most mRNAs encoding soluble proteins are targeted to ribosomes and translated in a non-localized manner in the cytoplasm (1). In contrast, mRNAs encoding secretory proteins have their translation halted and are transported (in concert with the ribosome) to the endoplasmic reticulum (ER)[1] so translation can be coupled with import of the protein into the ER (2). In contrast to these two well studied mechanisms of translation, some mRNAs are targeted to specific regions of the cell where they undergo localized translation (3–5). These mRNAs contain elements, usually located in their 3′-untranslated region, that bind to RNA-binding proteins that direct mRNA targeting. Translation of transported mRNAs is repressed during transport, and the repression is removed after arrival at the proper location (5, 6). This mechanism is important for determining cell fate and cell polarity (6). In neurons, transport of mRNA may allow for local translation at or near synapses (7). Indeed there is evidence for specific targeting and translation of a newly synthesized mRNA to activated synapses (8). Another use for mRNA transport in developing neurons is for localized translation in growth cones during neurite outgrowth (9–11).

The mechanism by which mRNAs are transported to axons and dendrites is unclear. One hypothesis is that mRNAs are transported by RNA granules that correspond at an ultrastructural level to a large amorphous collection of ribosomes (12). Although these granules have been characterized at the cellular level, there has been little molecular characterization of the granules. The mRNA-binding proteins Staufen (Staufen 1 and Staufen 2) are localized to granules, and levels of transported mRNAs are decreased by dominant negative mutants

[1] The abbreviations used are: ER, endoplasmic reticulum; DIV, days *in vitro*; BDNF, brain-derived neurotrophic factor, KIF5a, kinesin family 5a; CaMKII, calcium/calmodulin-dependent protein kinase 2; ZCBP, zip code-binding protein; hnRNP, heterogeneous nuclear ribonucleoprotein; Pur, purine-rich single-stranded DNA-binding protein; CCV, clathrin-coated vesicle; SYNCRIP, synaptotagmin-binding, cytoplasmic RNA-interacting protein; CGI, comparative gene identification; G3BP, Ras GTPase-activating protein Src homology 3 domain-binding protein; ELAV, embryonic lethal abnormal vision; DEAD, aspartate glutamate alanine aspartate; IEB, interleukin enhancer-binding factor; CFP, cyan fluorescent protein; YFP, yellow fluorescent protein; IMP, insulin growth factor II mRNA-binding protein; FMRP, fragile X mental retardation protein; DIG, digoxigenin; FISH, fluorescence *in situ* hybridization; E, embryonic day; RACK, receptor for activated C kinase; YB-1, Y box-binding protein 1; EM, electron microscopy.

From the ‡Département de Biochimie, ‖Département de Physiologie, and ‡‡Centre de Recherches en Sciences Neurologiques, Université de Montréal, 2900 Edouard-Montpetit, Montreal, Quebec H3C3J7, Canada, §Montreal Neurological Institute, McGill University, 3801 University, Montreal, Quebec H3A2B4, Canada, and **Canada Montreal Proteomics Centre, McGill University, 740 Dr. Penfield, Montreal, Quebec H3A1A4, Canada

Received, August 9, 2005, and in revised form, November 29, 2005
Published, MCP Papers in Press, December 12, 2005, DOI 10.1074/mcp.M500255-MCP200

© 2006 by The American Society for Biochemistry and Molecular Biology, Inc.
This paper is available on line at http://www.mcponline.org

Downloaded from https://www.mcponline.org by guest on October 20, 2020

of Staufen (13–15) or by small interfering RNA to Staufen (16). However, specific mRNAs enriched in these RNA granules have not been described. Recently using association with the motor protein KIF5a, components of an RNA granule that appears to be important for the transport of CaMKIIα mRNA have been identified (16); but although this granule was quite large, there was no evidence that it was associated with ribosomes.

Some specific mRNA-binding proteins have been implicated in RNA transport in neurons. Zip code-binding proteins (ZCBP1 and ZCBP2) are transported to neurites in chicken and mammalian neuronal cultures and help localize β-actin mRNA to dendrites and growth cones (17–19). Disrupting this transport blocks growth cone motility (17). hnRNP A2 has been shown to recognize a motif present in some transported mRNAs, and disruption of this interaction blocks some mRNA transport (20). Again it is unclear whether the transport of β-actin or hnRNP A2-bound mRNAs is in the presence or absence of ribosomes. CaMKIIα mRNA transport was blocked by RNA interference to a number of granule proteins including Pur α and Staufen (16).

RNA granules consist of ribosomes, transported mRNAs, RNA-binding proteins, and motors. Using this criteria, we report here the enrichment and proteome of an RNA granule purified by subcellular fractionation from E18 rat brain. Many of the proteins identified in the proteome have been implicated previously in RNA transport, and these proteins localize together in neurites together with ribosomes and mRNA.

EXPERIMENTAL PROCEDURES

RNA Granule Purification—The outline of the purification strategy is shown in Fig. 1*A*. It is a modification of a standard protocol used to purify clathrin-coated vesicles (CCVs) from adult brain (21). 300 E18 rat brains were homogenized in 10 volumes of buffer A (10 mM MES, pH 6.8, 0.5 mM EGTA, 1 mM $MgCl_2$) using a glass-Teflon homogenizer (10 strokes, 1500 rpm), and the homogenate (H) was centrifuged for 20 min at 17,000 $\times$ *g* in an SS-34 rotor (Sorvall DuPont). The resulting supernatant (S1) was collected and centrifuged at 56,000 $\times$ *g* for 1 h in a T-865 rotor (Sorvall). The pellet from this spin is P1. The pellets were resuspended with a glass-Teflon homogenizer (five strokes, 1500 rpm) in a total volume of 10 ml of buffer A followed by dispersion through a 25 5/8-gauge needle. The suspension was then mixed with 10 ml of buffer A containing 12.5% (w/v) each of Ficoll and sucrose and centrifuged for 20 min at 43,000 $\times$ *g* in an SS-34 rotor. The pellet from this spin is SGp. The supernatant was removed, diluted 1:5 in buffer A, and centrifuged for 1 h at 91,000 $\times$ *g* in a T-865 rotor. The pellet was resuspended with a glass-Teflon homogenizer (five strokes, 1500 rpm) in a total volume of 15 ml of buffer A and cleared by centrifugation at 19,000 $\times$ *g* for 10 min. The supernatant (SGs) was equally divided in two 7.5-ml aliquots, and each was placed into a 13-ml thin-wall centrifuge tube for a Sorvall AH-629 rotor. Each tube was then underlayered with 2.5 ml of buffer A prepared with D_2O containing 8% (w/v) sucrose and centrifuged for 2 h at 116,000 $\times$ *g* in an AH-629 rotor. The resulting pellet (called the CCV fraction) was resuspended in 0.5 ml of buffer A, and the samples were loaded onto 20–50% linear sucrose gradients prepared in buffer A. The gradients were centrifuged in an AH-629 rotor at 145,000 $\times$ *g* for 45 min and then fractionated from the bottom into 12 fractions of 1 ml each. Fraction 1 and the pellet were collected (called the RNA granule fraction), diluted 2-fold in buffer B (buffer A plus 60 mM EDTA), and placed on a second 20–50% linear sucrose gradient in buffer C (buffer A plus 30 mM EDTA). This gradient was centrifuged in an AH-629 rotor at 145,000 $\times$ *g* for 180 min, and 12 fractions of 1 ml each were collected. The total protein complement of each fraction was then resolved by SDS-PAGE following precipitation of the proteins with trichloroacetic acid.

Proteomic Techniques—Fractions were separated by SDS-PAGE, stained with Coomassie Blue, and cut into 48 horizontal gel slices with each slice processed for in-gel trypsin digestion and peptide extraction (22). The extracted peptide mixtures were separated and analyzed in an automated system by nanoscale LC Q-TOF MS/MS as described previously (22). After fragmentation in the MS/MS mode, the resulting spectra were analyzed on line in house by the software analysis program MASCOT (Matrix Science Ltd.) version 1.9.03 to identify tryptic peptide sequences that matched to the National Center for Biotechnology Information (NCBI) non-redundant mammalian protein database NCBI nr from March 2, 2003). The parameters used in the search were: enzyme, trypsin; one missed cleavage was allowed; the fixed modification was carbamidomethyl (Cys) and the variable modification was oxidation (Met); the peptide tolerance was $\pm$0.5 Da and the MS/MS tolerance was $\pm$0.5 Da; the charge was 1+; the experimental mass was monoisotopic; and the instrument parameter was ESI-Q-TOF. Protein identification was based on one or more peptides with a MASCOT score at or above the identity score (usually between 35 and 40). In addition, for proteins with only one identifying peptide or proteins with multiple unique peptides below the identity score, spectra were manually inspected for the presence of three clearly identified consecutive y ions as described previously (23). One identifying spectra for each protein is shown in the supplemental information. All retained proteins also matched approximately to the molecular weight of the gel slice from which the identification originated. Once a protein was identified using the criteria above, peptides were assigned to the protein regardless of MASCOT score if the peptides were the best match to the assigned protein based on MS/MS fragmentation. A similar rule was used for peptides that matched an accepted identification but were from an adjoining gel slice. All identified peptides, their scores, masses, and additional information can be found in the supplemental material. Although peptide counts are semiquantitative and depend on the number of tryptic peptides/protein and other technical issues (such as peptide extractability from the gel slice), when enough peptides are present, quantitative predictions can be made (23).

Immunoelectron Microscopy—For pre-embedding immunogold labeling, the CCV pellet was resuspended in buffer A containing the primary antibody. After an overnight incubation at 4 °C, the sample was diluted 30-fold with buffer A, centrifuged at 91,500 $\times$ *g* for 1 h, resuspended in buffer A, and fixed in 0.05% glutaraldehyde in buffer A for 30 min on ice. After fixation, the suspension was filtered onto Millipore membranes (0.1-μm pores). Membranes were then washed three times for 15 min in buffer A, incubated three times for 15 min in 3% bovine serum albumin/buffer A, and subsequently incubated with protein A-gold or goat anti-mouse-gold secondary antibody in buffer A for 30 min with mild agitation at room temperature. Membranes were washed four times for 15 min in buffer A and fixed in 2.5% glutaraldehyde/buffer A overnight at 4 °C. After three washes of 15 min in 0.1 M sodium cacodylate, pH 7.4, membranes were fixed with reduced osmium, dehydrated, and processed for EM. Pictures were taken at sections with gold particles present. All pictures were quantitated in a blinded fashion. First all structures on the picture were identified as either RNA granule, CCV, or other, and the area of these regions was calculated using NIH Image. Regions with no structures were then assigned by default to empty. Gold particles were then assigned to one of the four categories based on proximity to the identified structures.

Downloaded from https://www.mcponline.org by guest on October 20, 2020

Plasmid Construction—IMAGE clones were obtained for mouse SYNCRIP (IMAGE clone 5293527), mouse hnRNP C (IMAGE clone 3492858), mouse CGI-99 (IMAGE clone 3656382), mouse G3BP1 (IMAGE clone 3152563), human ELAV-like 4/HU-D (IMAGE clone 5286347), human DEAD box 3 (IMAGE clone 3617040), and human interleukin enhancer-binding protein 2 (IEB2) (IMAGE clone 4778612). Enhanced cyan fluorescent protein (CFP) and enhanced yellow fluorescent protein (YFP) (Clontech) were cloned into the pCDNA-RSV vector. Primers were designed to amplify the entire reading frame of the IMAGE clones, and these were inserted at the C terminus of enhanced CFP and enhanced YFP. Clones were sequenced and expressed in human embryonic kidney 293T cells to confirm that proteins were produced at the correct molecular weight using blotting with anti-fluorescent protein antibodies (data not shown).

Localization of Fluorescent Protein-tagged Proteins in Hippocampal Cultures—Primary hippocampal neuron cultures derived from E17–E19 Sprague-Dawley rat embryos (Charles River Laboratories) were cultured on 0.1% poly-D-lysine-coated round 18-mm diameter glass coverslips (Fisher) according to the standard protocol (24). Culture media consisted of Neurobasal medium supplemented with 1× GlutaMax, 25 μM glutamate, and 2% B27 supplements (Invitrogen). On day 3 after plating, one-half of the culture media was removed and replaced with fresh media without glutamate. On days 4–6 after plating, transfections were carried out with $CaPO_4$-DNA/Hepes buffered saline (pH 7.04) precipitate in fresh medium with 1 μg of total DNA/coverslip. Protein expression was assessed 16–20 h later. All DNA used for transfections was double-banded CsCl-purified. The transfected neurons were fixed in 4% paraformaldehyde in PBS containing 4% sucrose treated for immunocytochemistry and mounted with Prolong Antifade reagent (Molecular Probes). Images were acquired on a Nikon TE2000U inverted microscope using a 60× 1.4 numerical aperture objective, magnification of 1.5×, standard fluorescence cubes, and a Photometrics CoolSnap HQ (Roper Scientific) camera. Images were deblurred off line by a deconvolution protocol using a nearest neighbor point spread function (Metamorph, Universal Imaging).

Immunocytochemistry and Immunoblotting—The following primary antibodies were used: hnRNP A1 (generous gift of Dr. Gideon Dreyfus, University of Pennsylvania), SYNCRIP (generous gift of Dr. Akihiro Mizutani, Laboratory for the Brain Science Institute, RIKEN), IMP-2 (generous gift of Dr. Jan Christiansen, University of Copenhagen, Copenhagen, Denmark), YB-1 (generous gift of Dr. Nahum Sonenberg, McGill University, Montreal, Quebec, Canada), rabbit anti-S6 antibodies (Cell Signaling Technology), mouse monoclonal anti-Staufen 2 antibodies (25), human anti-P0 antibodies (a generous gift of Dr. Morris Reichlin, Oklahoma Medical Research Foundation), FMRP (Chemicon), Pur α/β (a generous gift of Dr. Kelm, Mayo Foundation), (26), and dynein (Santa Cruz Biotechnology). The antibody to DEAD box 3 was raised against the peptide CDKSDEDDWSKPLPPSER-amide after coupling to keyhole limpet hemocyanin-maleimide (Pierce). The antibody to CGI-99 was made using a GST-CGI-99 fusion protein as an antigen. As secondary antibodies, Alexa Fluor 594 goat anti-rabbit IgG, goat anti-mouse IgG, and goat anti-human IgG (dilution, 1:1000; Molecular Probes) were used. For immunoblotting, secondary antibodies linked to peroxidase (Pierce) were used, and imaging was obtained by enhanced chemiluminescence.

Fluorescence in Situ Hybridization with Digoxigenin-labeled Probes—23-mer poly(dT) were 3′ end-labeled with digoxigenin (DIG) as indicated by the manufacturer (Roche Applied Science). DIG incorporation was checked by dot blot. Fixed cells were subjected to fluorescence *in situ* hybridization (FISH) with the DIG-labeled poly(dT) probes as described previously (11). Hybridized probes and xFP fusion protein were detected by immunofluorescence using a sheep anti-DIG antibody (1:200; Roche Applied Science) and a mouse anti-green fluorescent protein (1:200; Roche Molecular Biochemicals). Secondary antibodies used were Alexa 594-conjugated anti-sheep IgG and Alexa 488-conjugated anti-mouse IgG (1:1000; Molecular Probes).

Live Cell Imaging of RNA Granules—Sixteen hours after transfection, YFP-DEAD box 3-expressing neurons were imaged with an upright laser scanning confocal microscope (Olympus BX51W1 and Bio-Rad MRC-600) and a long range water immersion objective (60×/0.90). Transfected cells were transferred to an opened perfusion chamber and maintained submerged at 35 °C in oxygenated (95% O_2, 5% CO_2) physiologic ACSF buffer (124 mM NaCl, 5 mM KCl, 1.25 mM NaH_2PO_4, 10 mM D-glucose, 2 mM $MgSO_4$, 26 mM $NaHCO_3$, 2 mM $CaCl_2$, and 0.05 mM Trolox) or depolarizing buffer (ACSF supplemented with 45 mM KCl) or BDNF (ACSF supplemented with 50 ng/ml BDNF) for never longer than 50 min perfused at 2 ml/min. Images were acquired every 30 s. The total number of puncta in neurites was measured in cells fixed after 30 min of BDNF, and the number of puncta/μm of neurite was measured using the threshold function of Image J.

Purification of mRNA and RT-PCR—RNA was purified using the RNAqueous-4PCR kit (Ambion, Austin, TX) according to the protocol provided by the manufacturer and converted to cDNA using Superscript. Specific forward primers and reverse primers were generated to the 3′-untranslated region of β- and γ-actin, dendrin, glucose-6-phosphatase, and CaMKIIα. The template was titered until amplification was linear (*i.e.* 2-fold more template led to 2-fold more amplified product). Dilutions of cDNA in this range were then amplified for 35 cycles, run on agarose gels, and stained with ethidium bromide. Images of gels were quantified with NIH Image. For each fraction (*e.g.* E18 brain, CCV, and RNA granule), a value was calculated based on the density of the band/ml of template added. The average value of this number over the three most linear dilutions was used for each fraction. For each fraction the value for β-actin was standardized to that of γ-actin (*i.e.* the value for β-actin was divided by the value for γ-actin). Finally the standardized values of β-actin for CCV and RNA granules were divided by the standardized value of β-actin from the E18 brain extract to determine the -fold enrichment of β-actin mRNA compared with γ-actin mRNA during the purification.

RESULTS

Purification of RNA Granules—This work initiated from a comparison of purified clathrin-coated vesicles (CCVs) from either embryonic E18 or adult brains. Examination of Coomassie-stained gels of these two preparations identified a number of bands that were enriched in E18 brains (Fig. 1*B*). These bands were isolated and sequenced using tandem mass spectrometry. They consisted of ribosomal proteins and of RNA-binding proteins including hnRNP A1, hnRNP A2, SYNCRIP, and IMP-2, the rat homologue of ZCBP. To investigate the possibility that these proteins were from a source distinct from CCVs, we performed electron microscopy on these preparations. The preparation from E18 brain contained a large number of structures that resembled amorphous collections of ribosomes, similar to what had earlier been described as RNA granules in brains (12, 14, 27) (Fig. 1*C*). The size (100–300 nm) and number of ribosomes per aggregate (20–100) match other characterization of these granules (27). These collections of ribosomes observed in the EM pictures did not resemble polyribosomes (beads on a string). The essentially identical protocol used on adult brain homoge-

Downloaded from https://www.mcponline.org by guest on October 20, 2020

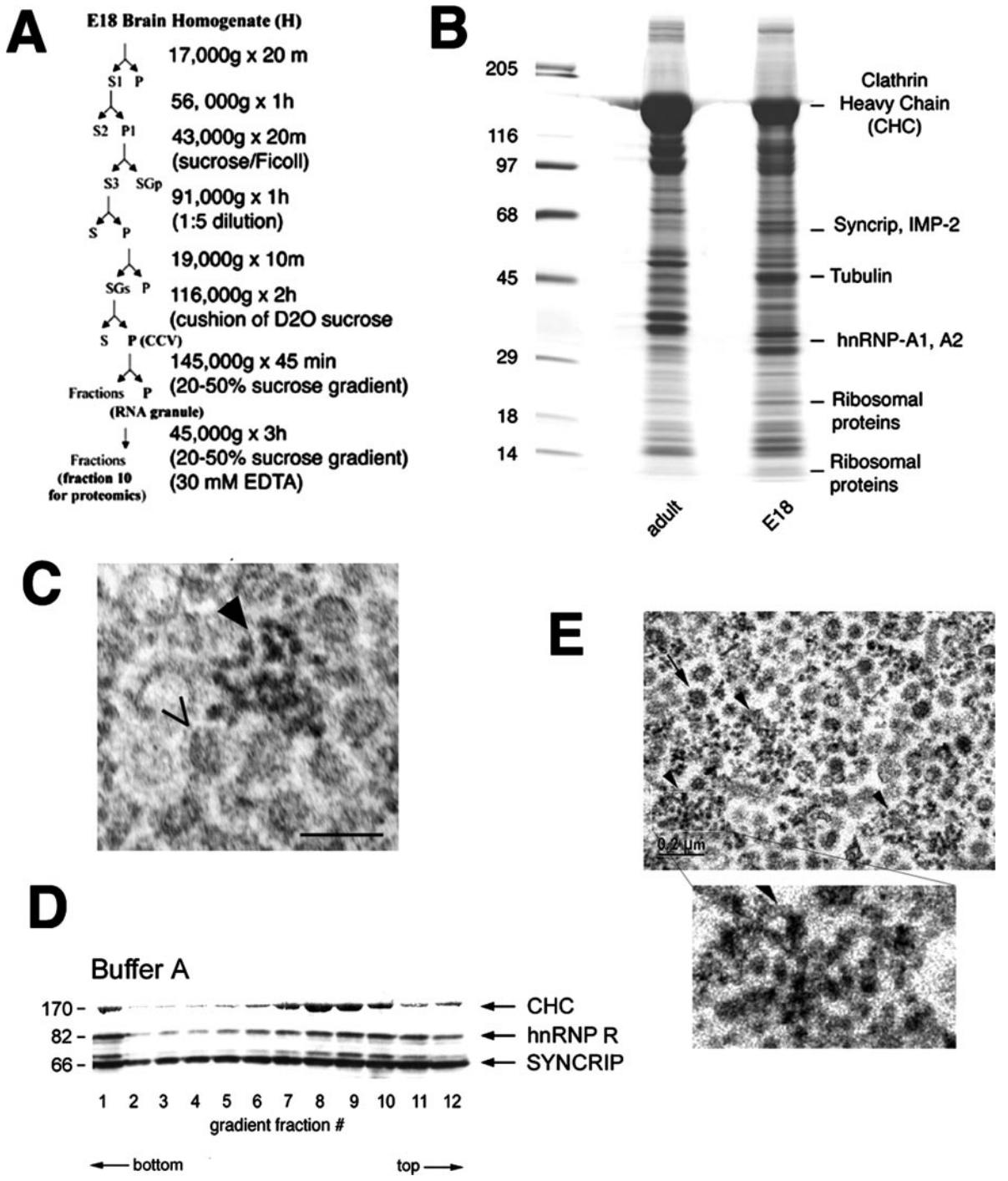

FIG. 1. **Isolation of an enriched RNA granule fraction.** *A*, schematic for the purification of the RNA granule fraction; details are under "Experimental Procedures." *B*, 100 μg of the CCV fraction from E18 and adult brains were separated by 5–15% gradient SDS-PAGE and Coomassie-stained. *Bars* represent bands excised from the E18 gel, and pertinent proteins identified by mass spectrometry are shown *beside* the *bar*. *C*, EM micrograph of the CCV fraction from E18 brain. The *dark filled arrowhead* points to a putative RNA granule, and the *outlined arrowhead* points to a CCV. *Scale bar*, 100 nm. *D*, the CCV fraction was separated on a sucrose gradient prepared in 100 mM MES, pH 6.5, 1 mM EGTA, and 0.5 mM $MgCl_2$ (buffer A). Fractions from the gradient were separated by SDS-PAGE (*1* = pellet and *12* = top), transferred to nitrocellulose, and processed for Western blot using antibodies against granule markers SYNCRIP and hnRNP R as well as a CCV marker, the clathrin heavy chain (*CHC*). *E*, EM micrograph of the pellet after sucrose gradient fractionation of the CCV fraction from E18 brains. *Arrowheads* point to putative RNA granules, and *arrows* point to CCVs; the *inset* shows higher magnification of a putative RNA granule.

Downloaded from https://www.mcponline.org by guest on October 20, 2020

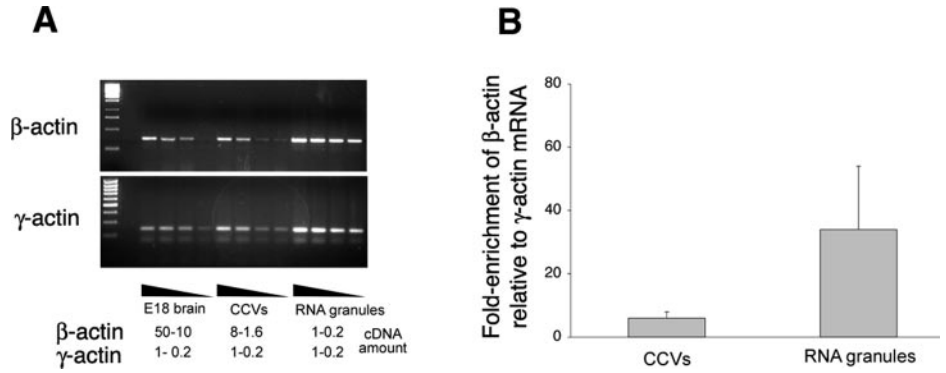

FIG. 2. **Enrichment of β-actin in the RNA granule fraction.** *A*, RT-PCRs were performed using RNA purified from E18 brains, CCV fractions, or isolated RNA granule fractions. Template cDNAs were serially diluted until a linear relationship between template amount and product amplification was observed. The range of template cDNA used for the four lanes from each fraction to obtain a linear amplification (μl) is indicated. Note that much more template obtained from E18 brains was required for amplification of the β-actin cDNA compared with the γ-actin cDNA, whereas similar amounts were needed for templates purified from the RNA granule fraction. *B*, quantification of three independent experiments as described in *A*. The enrichment of each mRNA was calculated independently based on E18 brain as a standard, and then a ratio of the enrichments was calculated to determine differences between levels of β-actin and γ-actin cDNA (see "Experimental Procedures" for detailed calculations).

nates or liver preparations contained 80–90% clathrin-coated vesicles (21, 23), and in these preparations we did not detect any amorphous collections of ribosomes. The presence of both mRNA-binding proteins involved in transport and ribosomal proteins suggest that in E18 brain this preparation may be enriched in an RNA granule. The morphology of the EM structures observed in this preparation is consistent with this hypothesis.

To further purify the RNA granule preparation from the CCVs and eliminate any possible polyribosomes, we used a 20–50% sucrose density gradient centrifugation and followed the RNA-binding protein fraction with antibodies to SYNCRIP. It has been demonstrated that RNA granules are separated from polyribosomes by this procedure (14). Western blotting analysis of each fraction of the gradient and of the pellet showed ~18 ± 3% (S.E., $n = 4$ preparations) of the SYNCRIP immunoreactivity in the pellet (Fig. 1*D*). Similar results were seen with other antibodies to RNA-binding proteins (data not shown), consistent with the sedimentation of RNA granules. Quantitative EM analysis (Fig. 1*E*) of the pellet from this sucrose gradient revealed that 47% ± 2% of the area had structures that resembled amorphous collections of ribosomes (see Fig. 1*E*, *inset*; 45 ± 2% CCVs and 7 ± 1% of other profiles; S.E.; $n = 20$ pictures, quantification by area). These experiments strongly suggest that the collections of ribosomes are not polysomes.

Transported mRNAs Are Enriched in the RNA Granule Fraction—If the pellet is indeed enriched in RNA granules, it should also be enriched in mRNAs undergoing transport. Although there are a number of mRNAs such as those coding for dendrin, microtubule-associated protein 2, and CaMKIIα that are enriched in dendrites of adult brain, few of these are known to be transported in developing brain. An exception is the mRNA for β-actin that is transported both in axons and dendrites of developing neurons (11, 18, 19). This mRNA was also shown to co-localize with RNA granules (12). To determine whether β-actin mRNA is enriched in the purified RNA granules, we compared RNA levels in homogenates from E18 brain, in the CCV fraction, and in the pellet after sedimentation through the sucrose gradient (RNA granule). β-Actin mRNA levels were determined in these fractions using semiquantitative RT-PCR, normalizing its expression to that of γ-actin mRNA, a non-transported mRNA (11). Much less template was needed to amplify β-actin mRNA from the RNA granule fraction than from the starting material, whereas there was no difference in the amount of template required to amplify γ-actin (Fig. 2, *A* and *B*). Thus, β-actin mRNA is enriched in the purified granule preparation compared with a non-transported mRNA γ-actin (Fig. 2, *A* and *B*). We also examined a number of other mRNAs in the CCV fraction including those coding for CaMKIIα, dendrin, and glucose-6-phosphatase. mRNA encoding dendrin was partially enriched in the CCV fraction (2-fold relative to γ-actin), whereas mRNA encoding glucose-6-phosphatase showed a profile similar to mRNA for γ-actin. The relative level of mRNA for CaMKIIα was decreased in the CCV fraction (5-fold less than γ-actin) perhaps due to the fact that at E18 very little CaMKIIα mRNA is expressed in neurons.

Final Purification of the RNA Granules—To generate the most enriched fraction with the least amount of contaminants, we further fractionated the pellet of the first sucrose gradient (RNA granule in Fig. 1*A*) on a second 20–50% sucrose gradient in the presence of EDTA. We noticed that under these conditions RNA granules components migrated more slowly into the gradient than did the CCVs. Indeed Coomassie staining and Western blotting (Fig. 3*A*) of the final fractionation demonstrated a peak of several RNA-binding proteins in fractions 9 and 10 with good separation from the peak of CCVs in fractions 3 and 4. It is interesting to note that protein bands

Downloaded from https://www.mcponline.org by guest on October 20, 2020

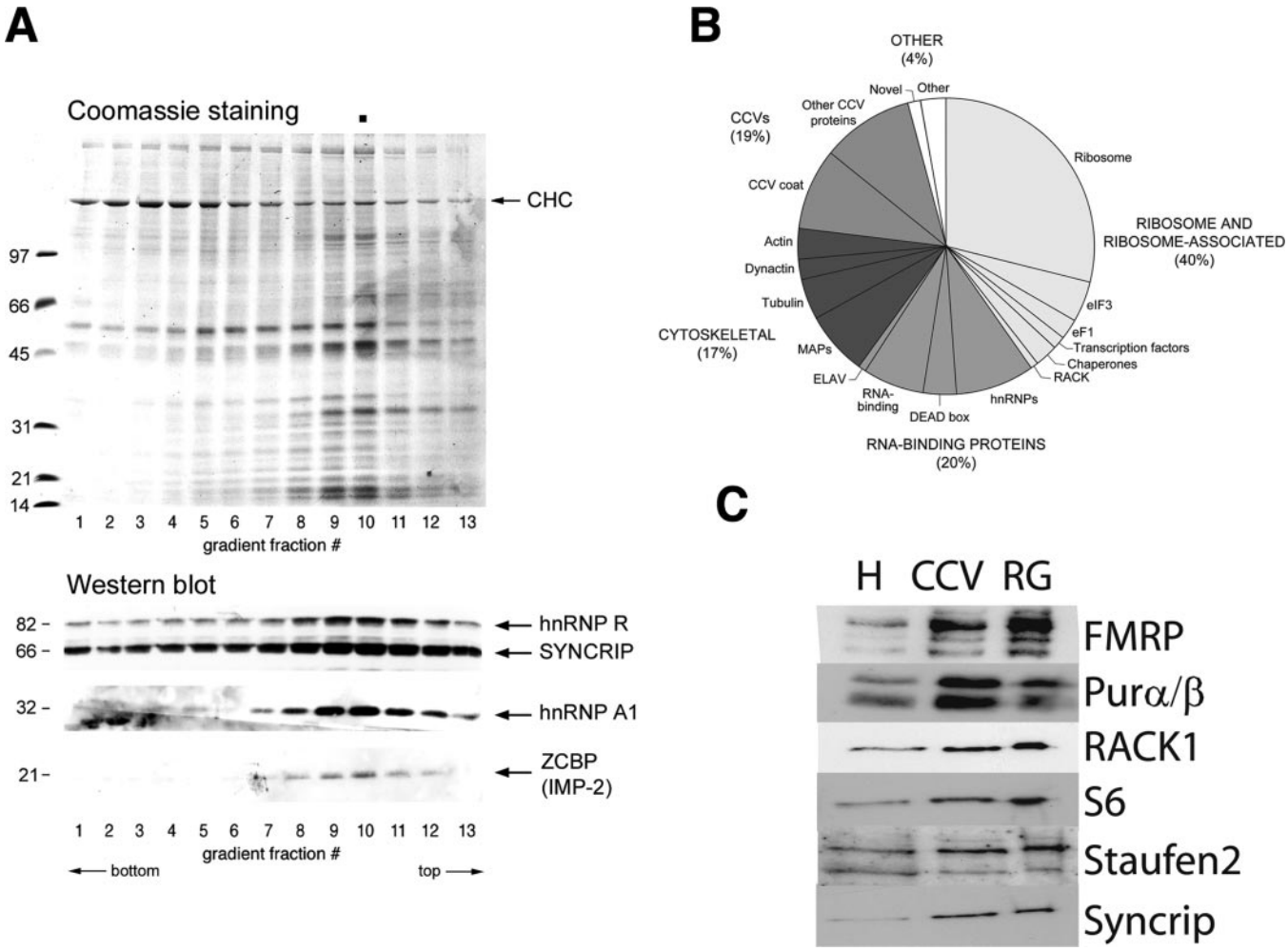

FIG. 3. **Proteomics of the RNA granule fraction.** *A*, the pellet from the first sucrose gradient run in buffer A (RNA granule) was resuspended in buffer A containing 30 mM EDTA and separated on a second gradient for 180 min (see "Experimental Procedures"). Proteins from all fractions were precipitated and separated by SDS-PAGE. Coomassie staining (*upper panel*) revealed a series of protein bands enriched in fractions 9 and 10. The *dot* marks the lane used for proteomic analysis. Positions of the clathrin heavy chain (*CHC*) and molecular weight markers are indicated. Immunoblots of the final fractionation (*lower panel*) against granule markers revealed enrichment of RNA-binding proteins in fraction 10. *B*, peptide counts for each class of proteins are shown in a pie chart. *C*, immunoblots for proteins identified in the proteomics and two proteins in RNA granules that were not identified in the proteomics (FMRP and Pur α/β) demonstrated their enrichment in the RNA granule fraction. 10 μg of E18 homogenate (*H*), CCV pellet (*CCV*), RNA granule (*RG*) are shown. *MAP*, microtubule-associated protein.

that peak in fractions 9 and 10 range from 10 to 500 kDa. The concentration of proteins of such variable size is consistent with the idea that they are associated in a large molecular mass complex.

Abundant Components of the RNA Granules—To this point, our experiments were consistent with the possibility that we had isolated a RNA granule. To further characterize this structure, we identified the abundant protein components of this fraction using tandem MS and then characterized the identified proteins as components of RNA granules in neurons. Their presence in processes in the form of puncta, their colocalization in common structures with ribosomes, the colocalization of mRNA, and their movement in dendrites would be further proof for our isolation of an RNA granule.

Fraction 10 from the final purification (Fig. 3*A*) was used to identify the abundant protein components of the RNA granule fraction. In total, using tandem MS, we identified 205 proteins (Supplemental Tables S1–S5). Approximately 80% of the proteins were ribosomal proteins or ribosome-associated proteins, RNA-binding proteins, and cytoskeletal proteins, consistent with a relatively pure preparation of RNA granules (Fig. 3*B*). Approximately 20% of the peptides identified were from CCV components as expected from our EM studies. The proteome of the CCV was recently described (23); it is relatively easy to separate these proteins from the RNA granule proteins. Importantly there were very few known contaminants: no mitochondrial proteins and no obvious nuclear contaminants (*i.e.* abundant histones, splicing factors, and lamins) were observed. Two proteins from the ER (immunoglobulin-binding protein (BIP) and an *N*-acetyltransferase) were observed.

Downloaded from https://www.mcponline.org by guest on October 20, 2020

The largest percentage of peptides in the proteomics derived from the ribosome (Fig. 3*B*), consistent with the appearance of the granule as a collection of ribosomes in EM (Fig. 1, *C* and *E*). The large number of RNA-binding proteins identified (46, see Supplemental Table S2) attest to the fact that these structures are not just pure ribosomes but also contain mRNA particles. Notably a number of these have been demonstrated previously to be present in transporting RNA structures in the brain (Table I, top). There are also a number of RNA-binding proteins that were identified that have never been associated with transporting structures (Table I, bottom). A large number of cytoskeletal components, including dynein and associated proteins, were identified as might be expected for a transporting organelle. It should be noted that some of the cytoskeletal components (especially actin and tubulin) are also present on CCVs from adult brain (Supplementary Table S3 and Ref. 23). A number of novel proteins that were previously identified only as open reading frames (Supplemental Table S4) were also identified in the granule fraction.

The ribosome is a good indicator of the completeness of the proteomics because its composition is well defined. We isolated 61 of 64 total ribosomal proteins over 10 kDa (proteins under 10 kDa were probably run off the gel), demonstrating the relative completeness of our analysis but also indicating that proteins that are undoubtedly present in our subcellular fraction were missed in the analysis. Two of the known RNA-binding proteins involved in transport were missing in our proteomics, FMRP and Pur α/β (16, 28, 29). The lack of FMRP is especially surprising because cytoplasmic FMRP-interacting protein, a known FMRP partner (30), was identified in the proteomics. To determine whether these proteins were indeed present in the granule fraction, we compared levels of FMRP and Pur α/β to several proteomically identified proteins in Western blotting of E18 brain homogenate, the CCV fraction, and the RNA granule (Fig. 3*C*). Pur α/β and FMRP were enriched to the same extent as other proteomically identified proteins suggesting the lack of peptides for these proteins was due to technical reasons, perhaps due to their presence in bands with abundant CCV components such as adaptins, poor tryptic cleavage, or other unknown factors.

Localization of Proteins to Granules Using Immuno-EM—To validate the assumption that the EM profiles that resemble amorphous collections of ribosomes are the source of the proteomically identified proteins, we used immuno-EM to assign specific proteins to CCVs, ribosome aggregates, or other components of the CCV fraction. The CCV fraction was incubated with primary antibodies, filtered onto nitrocellulose membranes, and then processed using secondary antibodies. It should be noted that because CCVs can pass through the filter used, the abundance of CCVs relative to ribosome aggregates and large membranous contaminants was reduced compared with that seen before filtration. The procedure also appeared to fragment the ribosome aggregates as the collections of ribosomes were generally smaller after the procedure

TABLE I

RNA-binding proteins identified in the proteomics

The table consists of RNA-binding proteins identified in the proteomics divided by class (hnRNPs, DEAD box helicases, ELAV-like proteins, and others). The top part lists proteins for which some published evidence implicates their presence in RNA granules (references given). The bottom part includes RNA-binding proteins for which there is no published evidence indicating their presence in RNA granules. Bolded proteins represent those examined in this study either by immuno-EM or localization of tagged proteins in hippocampal cultures. CYFIP, cytoplasmic FMRP-interacting protein; PTB, polypyrimidine tract-binding protein; ds, double-stranded; TAR, transactivation response region.

- RNA-Binding Proteins previously identified in RNA granules
  - hnRNPs
    - hnRNP D (Auf 1) (16)
    - **hnRNP A1** (16)
    - **SYNCRIP/hnRNP Q1/Gry-RBP** (16, 37)
    - hnRNP R1 (16)
    - hnRNP A/B (16)
    - hnRNP A2/B1 (20)
    - hnRNP A0 (16)
    - hnRNP U(16)
  - DEAD box helicases
    - **DEAD box 3** (16)
    - DEAD box 1/DDX1 (16)
    - DEAD box 5/17 (16)
  - Other RNA-binding proteins
    - ZCBP/IMP-2 (19)
    - Nucleolin (16)
    - **Staufen 2** (14, 16)
    - RNA granule protein 105 (45)
- RNA-binding proteins not previously identified in RNA granules
  - hnRNPs
    - hnRNP K
    - **hnRNP C**
    - TAR DNA binding
    - hnRNP L
    - hnRNP X (E2)
    - hnRNP H
    - hnRNPA3
    - hnRNP M
  - DEAD box helicases
    - DEAD box 6
    - DEAD box 9
    - NORP1 (regulator of nonsense)
    - eIF4A
    - DEAD box BAT-1
  - Other RNA-binding proteins
    - Zip code-binding protein 2/MARTA1
    - **G3BP1**
    - Nucleophosmin
    - Activator of dsRNA kinase
    - **Interleukin enhancer-binding factor 2**
    - Interleukin enhancer-binding factor 3
    - G3BP2
    - PTB
    - Poly(A)-binding protein
    - Matrin-3
    - PAI-1 RNA binding
    - **Y box-binding protein 1 (mYB-1b)**
    - CYFIP2
  - ELAV-like proteins
    - ELAV-like 2 (Hu-B)
    - **ELAV-like 4 (Hu-D)**
    - ELAV-like 3 (Hu-C)
    - ETR-R3B

Downloaded from https://www.mcponline.org by guest on October 20, 2020

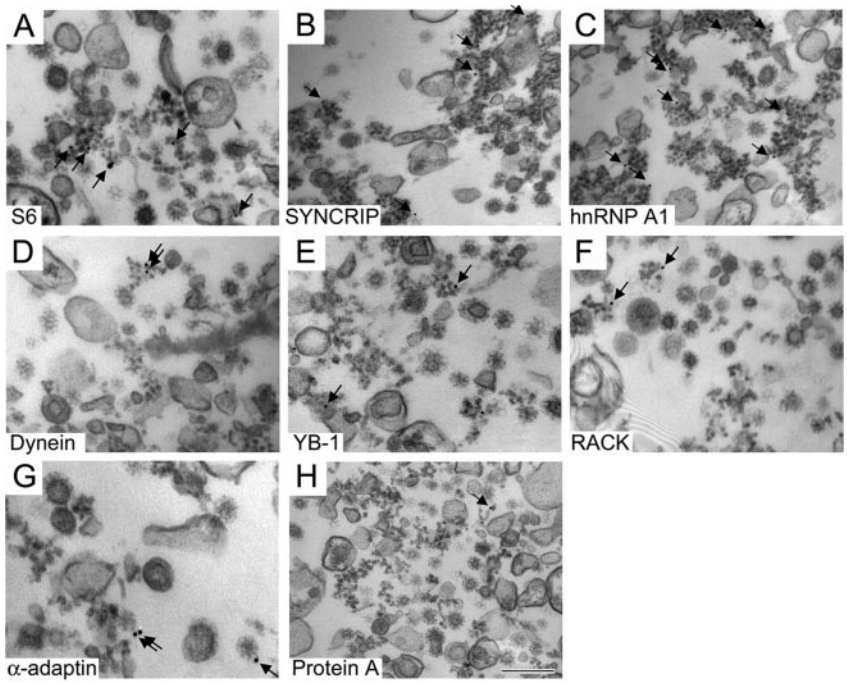

FIG. 4. **Localization of selected proteins in crude CCV fractions using immuno-EM.** *A–H*, granules are evident as clusters of *round dots*, whereas CCVs are obvious due to their coats. *Arrows* point to gold particles. The antibody used is given *underneath* the EM plate. Protein A-gold alone was used as a control for rabbit polyclonal antibodies. The goat anti-mouse-gold secondary antibody showed no background (not shown). The *scale bar* represents 200 nm. *I*, quantitation of immuno-EM. Values are S.E. of 10–30 EM micrographs from one to three different purifications.

I

	RNA Granules		CCVs	
Antibody	Density (Gold/Area)	% of Gold	Density (Gold/Area)	% of Gold
S6	**14 ± 4**	**52 ± 5**	0.4 ± 0.2	8 ± 3
SYNCRIP	**10 ± 2**	**55 ± 9**	0.7 ± 0.3	6 ± 4
hnRNP A1	**7 ± 2**	**48 ± 6**	2 ± 0.9	15 ± 4
Dynein	**12 ± 2**	**46 ± 5**	1 ± 0.5	4 ± 1
YB-1	**15 ± 2**	**34 ± 5**	1.3 ± 0.4	8 ± 3
RACK	**5 ± 1**	**51 ± 4**	0 ± 0	0 ± 0
α-adaptin	1 ± 0.4	6 ± 3	**10 ± 1**	**68 ± 6**
Protein A	1 ± 1	15 ± 5	0.6 ± 0.4	4 ± 2

than seen earlier (*i.e.* Fig. 1*C*). As controls, antibodies to the ribosomal protein S6 (for putative RNA granules) and to the protein α-adaptin (for CCVs) were used (Fig. 4, *A* and *G*). All micrographs were quantitated using density of gold/structure as well as percentage of gold/structure. As expected, the ribosomal protein S6 was enriched in granule-like structures (Fig. 4, *A* and quantitated in *I*). Similarly the RNA-binding proteins SYNCRIP, hnRNP A1, and YB-1 were enriched on structures resembling RNA granules (Fig. 4, *B*, *C*, and *E* and quantitated in *I*). RACK was also highly associated with these structures (Fig. 4*F*), confirming earlier reports suggesting that RACK is a ribosome-associated protein in developing neurons (31) and that RACK and its homologue in yeast are associated with ribosomes (32, 33). Dynein showed the same degree of enrichment on the RNA granules as the RNA-binding proteins (Fig. 4, *D* and quantitated in *I*), demonstrating that dynein is a component of these structures. This result validates the identification of other members of the dynein complex (dynactin, centractin, and dynamitin) as abundant components of the RNA granules (Supplemental Table S3). This is consistent with evidence for dynein-dependent transport of RNA in other systems (34–36). As expected, α-adaptin was enriched in the CCVs (Fig. 4*G*), whereas protein A was not enriched in either structure (Fig. 4*H*). These experiments show that several of the proteomically identified proteins are associated with ribosome aggregates, supporting the possibility that they are components of RNA granules.

Proteomically Identified Proteins Form Puncta in Dendrites of Hippocampal Neurons—To further characterize the RNA granule preparation, we expressed CFP- or YFP-tagged versions of seven of the proteomically identified proteins in hippocampal neurons. We chose a number of proteins that had not been shown previously to be part of RNA granules at the time of this analysis and that yielded relatively large numbers of peptides during tandem MS analysis, including DEAD box 3, SYNCRIP, hnRNP C, G3BP1, ELAV-like 4, IEB2, and CGI-99 (Fig. 5*A*). We used a relatively weak promoter (Rous sarcoma virus) and looked early after transfection (16–20 h) to minimize effects of overexpression. We used hippocampal cultures that were still in a growth phase (4–5 DIV) to match the developmental state from which the granules were isolated (E18). Whereas YFP (Fig. 5*B*) or CFP (data not shown) were completely diffuse, the tagged proteins revealed strong staining in cell bodies as well as prominent puncta in neurites (Fig. 5, *D–Q*). YFP-DEAD box 3 showed the most neuritic puncta in dendrites. Most of the other expressed proteins

Downloaded from https://www.mcponline.org by guest on October 20, 2020

A

Name	Peptides	Description	Reference
DEAD box 3/PL10	17	RNA helicase	50
SYNCRIP/hnRNP Q1/Gry-RBP	16	Cytoplasmic hnRNP, synaptotagmin-binding protein	55,56
G3BP1	12	RNA endonuclease, possible effector of RasGAP	57
ELAV-like 4/Hu-D	5	RNA stabilization protein	58,59
interleukin enhancer-binding factor 2 IEB2/NF45	3	RNA-binding protein, part of a complex containing dsRNA-binding protein IEB3/NF90	60,61
hnRNP C	3	Nuclear hnRNP	62
CGI-99	6	Novel protein	44

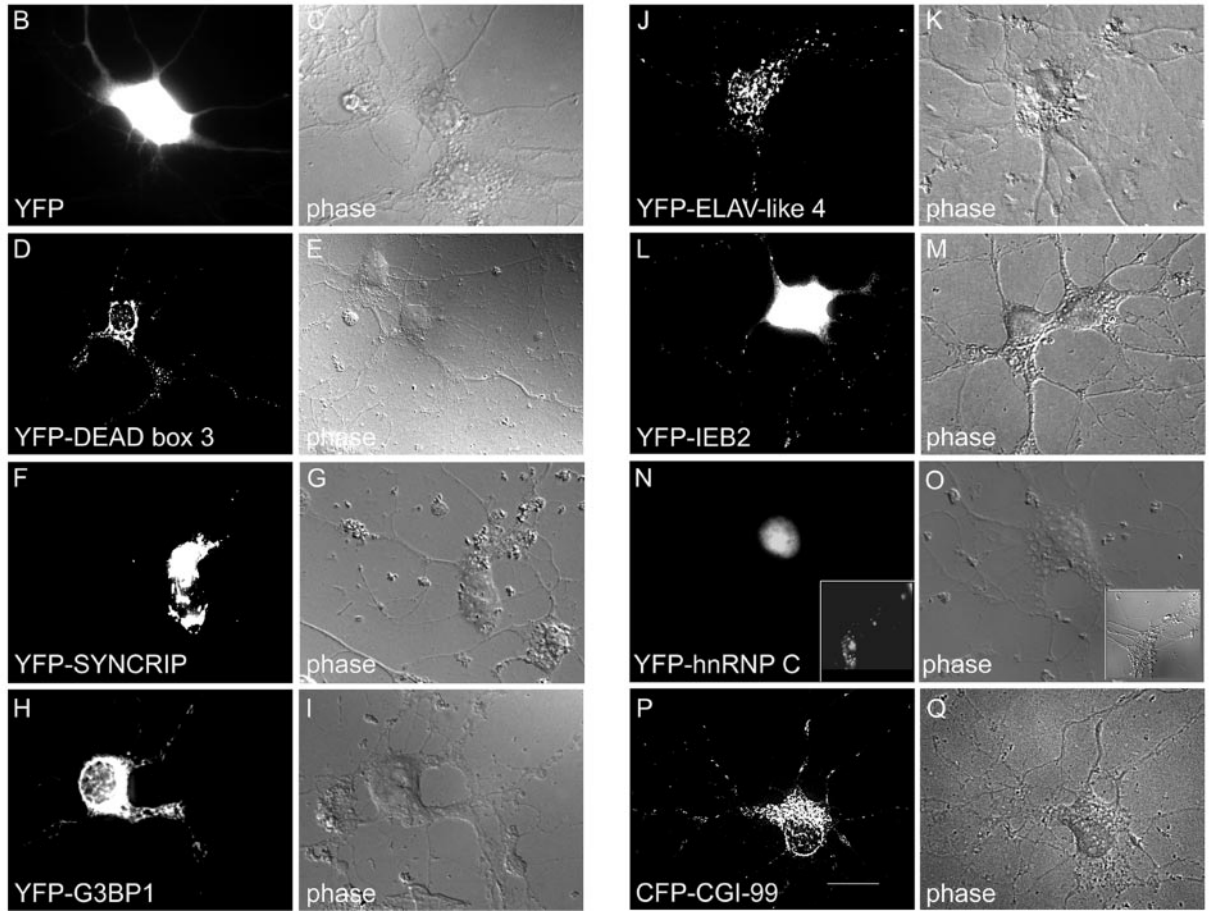

FIG. 5. **Expression of tagged fusion proteins in rat hippocampal neurons.** *A*, proteins were selected based on their abundance in the proteomics and their representation of a specific class. *B–Q*, YFP- or CFP-tagged proteins were transfected into 6-day hippocampal neuron cultures and then fixed the next day. Images were overexposed to visualize puncta in the processes. *Insets* in *N* and *O* show CFP-hnRNP C in neurites when overexposed. The *scale bar* represents 20 μm.

showed clear nuclear staining as well. One of them, hnRNP C, was mainly nuclear (Fig. 5, *N* and *O*), although in some neurons there were neuritic puncta visible after overexposure of the picture (see Fig. 5, *N* and *O*, *inset*).

To extend these results to the endogenous proteins, we raised antibodies to DEAD box 3 and to CGI-99. These antibodies each recognized a single band after Western blotting of brain extracts, and this band was greatly enriched in the CCV and RNA granule fractions (Fig. 6, *A–C*). When used for immunocytochemistry, puncta were observed in the cell body (Fig. 6, *D* and *H*) and neurites (Fig. 6, *E* and *I*) with the immune sera for each antibody but not with the preimmune sera (Fig. 6, *F*, *G*, *J*, and *K*). Thus, endogenous DEAD box 3 and CGI-99 are also found as puncta in neurites of hippocampal neurons.

Proteomically Identified Proteins Co-localize in Puncta—To determine whether proteomically identified proteins are components of common structures/puncta, CFP- or YFP-tagged-proteins were co-expressed in hippocampal neurons, and

Downloaded from https://www.mcponline.org by guest on October 20, 2020

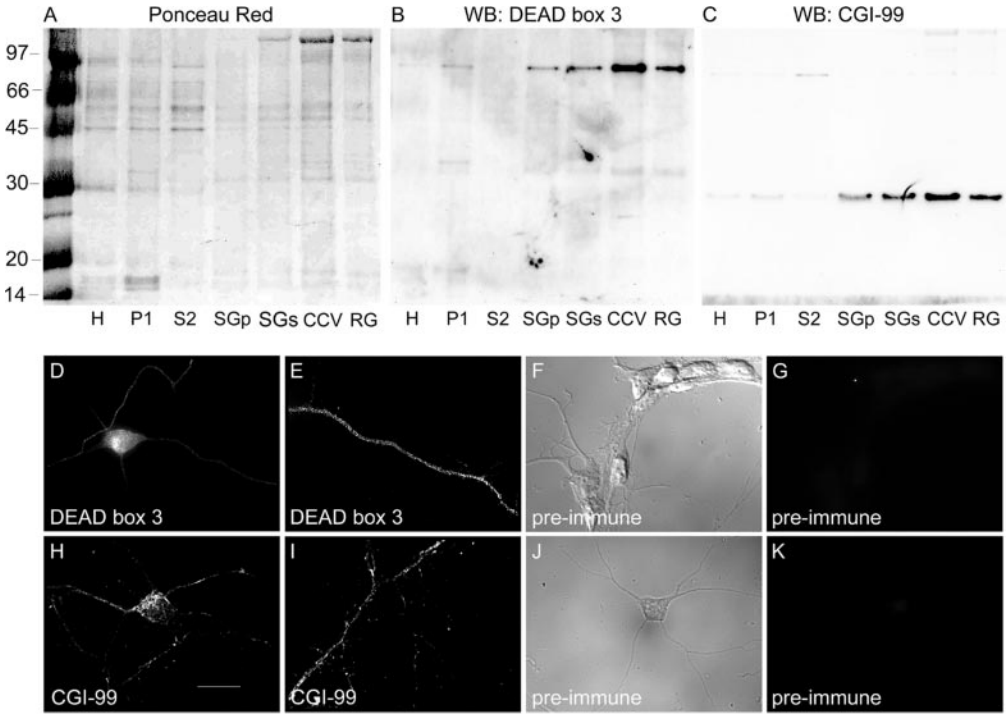

FIG. 6. **Expression of endogenous DEAD box 3 and CGI-99.** *A*, 10 mg from steps of the purification of RNA granules were separated on an SDS-polyacrylamide gel, transferred to nitrocellulose, and stained with Ponceau Red (*A*) or immunoblotted with antibodies raised to DEAD box 3 (*B*) or CGI-99 (*C*). *H*, homogenate; *P1*, pellet 1; *S2*, supernatant 2; *SGp*, sucrose gradient pellet; *SGs*, sucrose gradient supernatant; *RG*, RNA granules (pellet after 20–50% sucrose gradient in buffer A). For schematic and definition of fractions see Fig. 1*A* and "Experimental Procedures." The blots illustrate the enrichment of DEAD box 3 and CGI-99 in CCVs and RNA granules as well as the labeling of only a single band. Immunostaining of day 6 hippocampal cultures illustrates cell body and neuritic staining with the DEAD box 3 antibody (*D* and *E*) and with the CGI-99 antibody (*H* and *I*) and no staining when using the appropriate preimmune serum (*F*, *G*, *J*, and *K*) under the same conditions. The *scale bar* represents 20 μm. *WB*, Western blot.

their localization was observed by confocal microscopy. YFP-DEAD box 3 puncta contained most of the other proteomically identified proteins, although the levels of co-localization varied with different proteins (Fig. 7, *A–F*, and Table II). The lowest level of co-localization was observed with DEAD box 3 and CGI-99. However, CGI-99 strongly co-localized with several of the other proteomically identified proteins (Fig. 7, *G–J*, and Table II). The DEAD box 3 puncta showed only partial co-localization with Staufen 2 (Fig. 8, *G–I*, and Table II), a well characterized RNA-binding protein involved in RNA transport. CGI-99 also showed only partial co-localization with Staufen 2 (Table II and data not shown). Our results show that several proteomically identified proteins are components of the same puncta, consistent with these puncta being RNA granules. In addition, these experiments indicate that there are multiple types of RNA transport structures with overlapping subsets of the identified proteins.

DEAD Box 3 Co-localizes with RNA and Ribosome-containing Structures in Processes—We determined whether proteomically identified proteins co-localize with ribosomes in processes of hippocampal neurons and whether they contain RNA as would be expected for RNA granules. For the first task, an antibody to P0, a protein component of the large ribosomal subunit, was used as a marker for ribosomes. We focused on DEAD box 3 as it is the most punctate of the expressed proteins and is co-localized with most of the other proteomically identified proteins. Expressed DEAD box 3 protein co-localized with P0 (Fig. 8, *A–C*), although this co-localization was not complete. There were clearly subsets of DEAD box 3 puncta that did not contain P0 suggesting that the formation of RNA granules is dynamic and/or that DEAD box 3 plays multiple roles in neurons. Similarly subsets of P0 puncta did not contain DEAD box 3 (Table II), consistent with the heterogeneity of the RNA granule population. The DEAD box 3 granules also co-localized with S6, a protein of the small ribosomal subunit (data not shown). Using the anti-DEAD box 3 antibody, we found that the endogenous DEAD box 3 protein also co-localized with P0 although to a lesser extent than did the expressed protein (Fig. 8, *D–F*, and Table II).

To determine whether DEAD box 3 puncta also contained poly(A) mRNA, hippocampal neurons were transfected with YFP-DEAD box 3 and labeled with poly(dT) probe using FISH. As shown in Fig. 8 (*J–L*), both signals co-localized demonstrating that DEAD box 3-containing puncta carry poly(A) mRNA. The presence of puncta containing DEAD box 3, ribosomes, and poly(A) mRNA is strong evidence that this protein is a component of RNA granules. The co-localization of DEAD box 3 with the other proteomically identified proteins in these

Downloaded from https://www.mcponline.org by guest on October 20, 2020

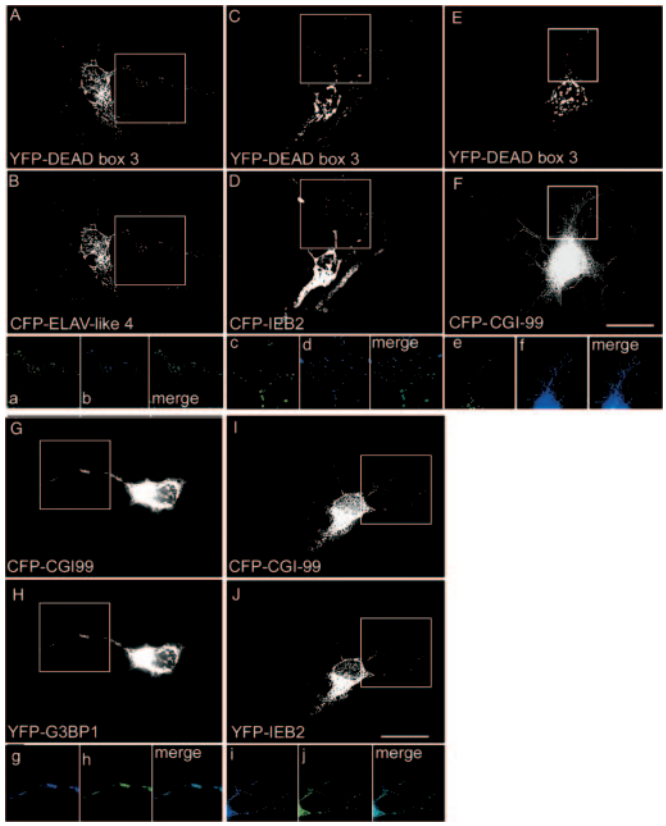

FIG. 7. **Co-localization of novel RNA granule components.** *A–J*, cultured hippocampal neurons were co-transfected with YFP-DEAD box 3 (*A*, *C*, and *E* and *a*, *c*, and *e*) and either CFP-ELAV-like 4 (*B* and *b*), CFP-IEB2 (*D* and *d*), or CFP-CGI-99 (*F* and *f*). Neurons were co-transfected with CFP-CGI-99 (*G*, *g*, *I*, and *i*) and either YFP-G3BP1 (*H* and *h*) or YFP-IEB2 (*I* and *i*). *Boxed regions* are in *green* (YFP; *a*, *c*, *e*, *h*, and *j*), in *cyan* (CFP; *panels b*, *d*, *f*, *g*, and *i*), and in *aqua* to show co-localization (*merge*). The *scale bar* represents 20 μm.

puncta argues strongly that the structures used for the identification of these proteins were indeed RNA granules.

DEAD Box 3 Puncta Move in Dendrites, and the Number of Moving Puncta Is Affected by BDNF but Not Activity—RNA transport structures have been characterized extensively using their speed and direction of transport (13, 16, 19, 37–39). Using YFP-tagged DEAD box 3, we imaged granule movement in living dendrites of cultured hippocampal neurons. As described for RNA granules, some DEAD box 3 granules moved in an oscillatory manner, and others moved in a single direction anterogradely or retrogradely (Fig. 9, *A–C*). The speed of the YFP-DEAD box 3 granules (0.03–0.1 μm/s; Fig. 8*D*) was similar to that measured for Staufen 1 granules (13) and CaMKIIα mRNA-containing granules (39) but slower than that measured for granules containing ZCBP (19). Similar to other measurements of RNA granules (19, 39), most of the puncta were nevertheless immobile. To test a putative regulation in the transport of these granules by cell activity, we compared the movement and speed of the granules when transfected hippocampal neurons were treated or not with KCl. KCl depolarizes neurons and mimics neuronal cell activity. Activity induced by KCl did not change the overall speed of the granules (Fig. 9*D*) or the percentage of granules that moved in an anterograde direction (Fig. 9*E*). Neurotrophins have been shown previously to increase the percentage of moving granules (40) and to increase transport of specific mRNAs (17, 41). We found that the neurotrophin BDNF significantly increases the percentage of moving YFP-DEAD box 3 puncta in cultured hippocampal neurons but does not affect their average speed (Fig. 10). We also observed an increase in the number of YFP-DEAD box 3 puncta in neurites 30 min after BDNF treatment (20.94 $\pm$ 2.26 puncta/50 μm in neurites with BDNF; $n = 52$ neurites in 13 neurons, compared with 12.79 $\pm$ 1.33 puncta/50 μm in control neurites; $n = 48$ neurites in 12 neurons, $p < 0.01$ Student's t test), consistent with the increased motility of these granules and thus their increased transport from the cell body.

DISCUSSION

Proteome of an RNA Granule from Developing Brain—Proteomics is usually thought of as a tool to use on highly purified fractions to determine the protein components of that fraction. Indeed this strategy has been used effectively to determine novel protein constituents of well characterized subcellular compartments such as CCVs, phagosomes, the nuclear pore, and many other aspects of cellular machinery (42, 43). However, in this case we used proteomics to gain additional tools for exploring the hypothesis that we had successfully isolated an RNA granule from E18 brains. Identification of proteins allowed us to characterize RNA granule components in hippocampal neurons at the cellular and molecular levels. Although highly enriched in structures described as amorphous collections of ribosomes, the fraction used for the proteomic analysis was not completely pure and contained another type of structures, the CCVs. Because the proteome of the CCV is well known, we could then determine the components of the amorphous collection of ribosomes. The abundance in the proteomics of ribosomal proteins, of RNA-binding proteins already implicated in transport (hnRNP A1, hnRNP A2, and ZCBP), and of the transport motor dynein strongly supports the identification of this structure as an RNA granule. Consistently a subset of the proteomically identified proteins was shown to be present in the structures identified in the EM as RNA granules (Fig. 4). The proteomics also eliminated several alternative possibilities for the structures due to the absence of nuclear matrix or spliceosome components. This was important because hnRNPs, the most abundant class of RNA-binding proteins found in the proteomics, are also components of nuclear granules involved in splicing. The lack of markers for other abundant subcellular compartments such as ER and mitochondria demonstrated the relative enrichment of this fraction over an extract.

The presence of several of the proteomically identified proteins in neurites of hippocampal neurons in the form of

Downloaded from https://www.mcponline.org by guest on October 20, 2020

TABLE II

Co-localization of proteomically identified proteins

For each co-localization, 5–25 cells were examined. The first column shows the co-expressed marker; fluorescently tagged expressed protein was used for all except for poly(dT) where FISH was used and for Staufen 2 and P0 where antibodies were used. The second column shows percentage of expressed DEAD box 3 puncta that contained staining for the other marker. The reciprocal column represents the percentage of puncta with the other marker that co-localized with expressed DEAD box 3. The next two columns show similar results for expressed CGI-99. ++, >60% co-localization; +, 30–60% co-localization; +/−, 10–30% co-localization; −, <10% co-localization; NA, not applicable; ND, not determined.

Co-localized marker	Expressed CFP- or YFP-DEAD box 3	Expressed CFP- or YFP-DEAD box 3 reciprocal	Expressed CFP-CGI-99	Expressed CFP-CGI-99 reciprocal
ELAV-like 4	++	++	+/−	+/−
G3BP1	++	++	++	++
hnRNP C	+/−	++	ND	ND
IEB2	++	+	++	++
CGI-99	+/−	+/−	NA	NA
Poly(dT) (FISH)	++	+	ND	ND
Staufen 2	+/−	+/−	+/−	+/−
DEAD box 3	NA	NA	+/−	+/−
P0	+ (+/− for endogenous DEAD box 3)	+/− (+/− for endogenous DEAD box 3)	ND	ND

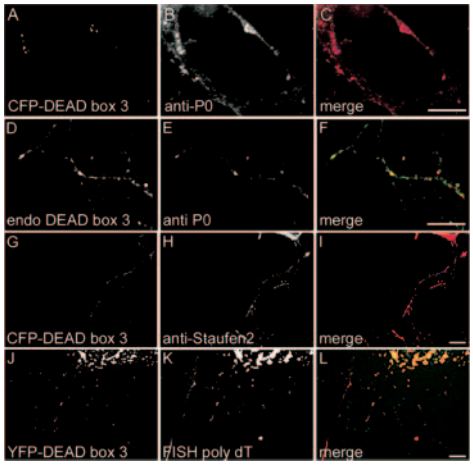

FIG. 8. **Co-localization of DEAD box 3 puncta with previously identified granule components.** Cultured hippocampal neurons at 6 DIV expressing tagged DEAD box 3 (*A*, *G*, and *J*) or immunostained with endogenous DEAD box 3 (*D*) were stained with P0 (*B* and *E*) or Staufen 2 (*H*) antibodies or processed with FISH for poly(dT) (*K*). Blended images show co-localization in *purple* (*merge*; *C* and *I*) or *yellow* (*merge*; *F* and *L*). The *scale bar* represents 20 μm.

puncta, their co-localization in structures that also contain ribosomes and poly(A) RNA, and their movement in processes at the same speed as that found in previous studies on RNA granules all add strong support to the assumption that we isolated and studied an RNA granule population. Other support comes from the comparison of our proteome with other published analyses of RNA granules. First, proteins initially not implicated in RNA transport before our proteomic analysis was done were subsequently implicated in RNA transport in neurons. This includes specific identifications such as SYNCRIP (37) and RNA granule protein 105 (45). Second, comparison with an RNA granule purified from adult brain on the basis of its association with the motor protein kinesin KIF5a (16) shows that many components are shared by the two preparations, including hnRNPs A0, A1, A/B, D, and U; SYNCRIP, nucleolin; FMRP; Pur α/β; DEAD boxes 1, 3, and 5; Staufen; EF1-α; and CGI-99. Several of the components have been shown to be required for transport of CaMKIIα mRNA in dendrites (16). This overlap serves as a validation for both screens due to the independent identification of a number of proteins not shown to be involved previously in RNA transport. However, there were also some differences in the compositions of these granules. The granules we isolated from developing brain are greatly enriched in ribosomes, whereas the KIF5a-containing granules from adult brain appear to lack a ribosomal component. Accordingly our EM studies did not detect amorphous collections of ribosomes in CCV preparations from adult brains (data not shown) suggesting that the RNA granules that we identified are greatly enriched during development. However, it does not exclude the presence of ribosome-associated RNA granules in adult brains because other studies, using different purification protocols, have identified RNA granules consisting of ribosomes from adult brain (27). It should be noted that despite the lack of detection of RNA granules using ultrastructural techniques, tandem MS results still identified some of the RNA granule proteins in adult CCV preparations (23).

Other differences were noted in the composition of our granule preparation and the KIF5a preparation (16). The granules that we isolated were enriched in proteins of the dynein complex, whereas the granule isolated by Kanai *et al.* (16) was based on its association with kinesin. The granule we isolated contains the actin-binding protein ZCBP, consistent with the enrichment for β-actin mRNA in the preparation, and a number of additional RNA-binding proteins not identified in the KIF5a granule including IEB2 and -3, ELAVs, and G3BP1 and -2. On the other hand, CaMKIIα mRNA was shown to be a major RNA associated with the KIF5a granules. This RNA was

Downloaded from https://www.mcponline.org by guest on October 20, 2020

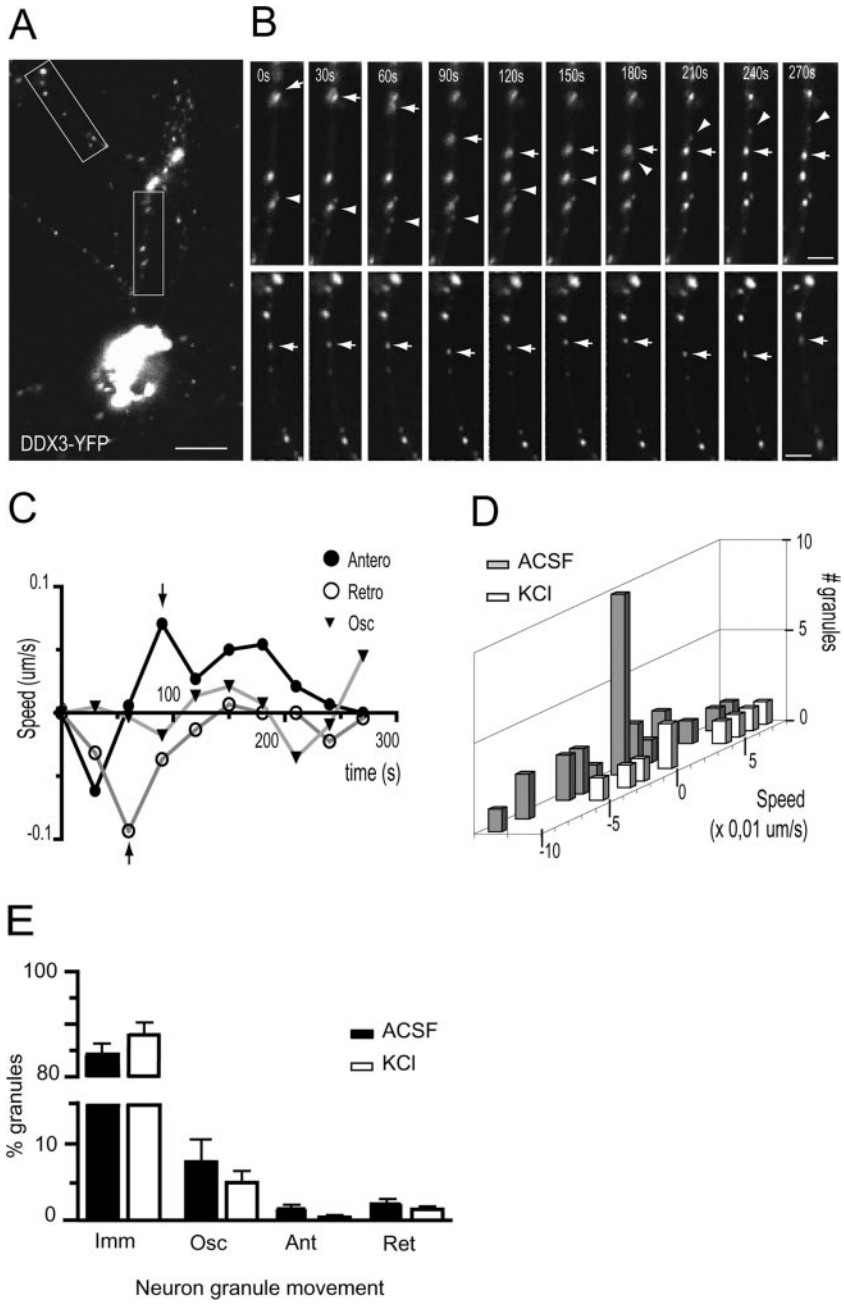

FIG. 9. **Movement of YFP-tagged DEAD box 3 granules.** *A*, a 7 DIV hippocampal neuron transfected with YFP-DEAD box 3. *Scale bar*, 10 μm. *B*, time lapse movies of the two *rectangular regions* of interest indicated in *A*. An example of granule movements for 270 s with 30-s intervals is shown. *Top*, granules moving retrogradely (*arrow*) and anterogradely (*arrowhead*). *Bottom*, a granule moving in an oscillatory fashion is also illustrated. *Scale bar*, 2 μm. *C*, graph of the displacement over time for the three granules from *B*. Maximal speeds are shown by *vertical arrows*. *D*, maximal speed from 20 granules in ACSF (*left*; *gray*) or 45 mM KCl (*right*; *white*). *E*, histogram of granule movement from five different neurons in ACSF (*black*) or 45 mM KCl (*white*).

not enriched in our granules. We hypothesize that the granules isolated from developing brain may be more involved in neurite growth, whereas the granules isolated from adult brains are more devoted to transporting dendrite-specific messages like CaMKIIα mRNA to the dendrites. This may be why neuronal activity mimicked by KCl did not affect the speed or direction of the granules because neurons at this stage are not highly electrically active. This is in contrast to granules that transport CaMKIIα mRNA that are regulated by activity (39). Because we showed that the granules form a heterogenous population, we do not exclude the possibility that other RNA granules may be regulated by neuronal activity in developing brains. Indeed ZCBP recruitment and movement in dendrites of cultured embryonic neurons was affected by KCl (19). Its transport is faster than that observed in our study, but it was observed at a later stage of neuronal culture (>14 DIV) (19). In contrast, we did observe an effect on granule movement by BDNF. An earlier report demonstrated that NT-3 increased the number of puncta and the number of moving puncta in cultured neurons using a nonspecific marker of granules, the RNA-binding dye SYTO-14 (40). Here we report similar results using a different neurotrophin, BDNF, and a specific marker of RNA granules, DEAD box 3. Neurotrophins have also been reported to affect RNA transport of

Downloaded from https://www.mcponline.org by guest on October 20, 2020

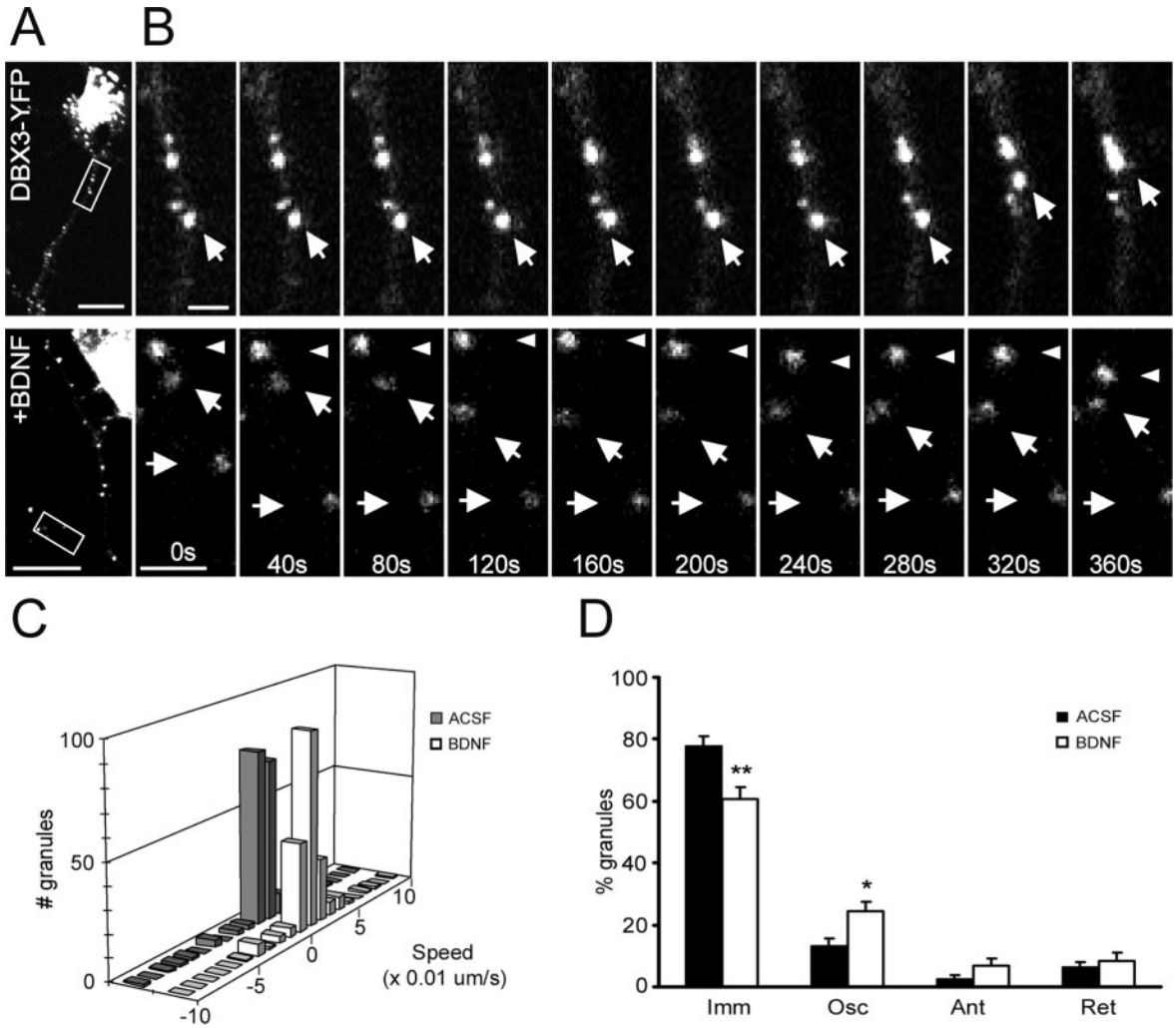

FIG. 10. **BDNF increases motility of YFP-tagged DEAD box 3 granules.** *A*, a 7 DIV hippocampal neuron transfected with YFP-DEAD box 3 and either non-treated or treated with 50 ng/ml BDNF for 15 min prior to imaging. *Scale bar*, 10 μm. *B*, time lapse movies of the two *rectangular regions* of interest indicated in *A*. An example of granule movements for 270 s with 30-s intervals is shown. Granules moving anterogradely and retrogradely (*arrow*) or in an oscillatory motion (*arrowhead*) are shown. *Scale bar*, 2 μm. *C*, maximal speed from 178 granules in ACSF (*gray*) or 187 granules in BDNF (*white*). *D*, histogram of granule movement from 18 different neurons in ACSF (*black*) or BDNF (*white*). * represents $p < 0.05$, unpaired Student's *t* test between control and BDNF.

β-actin (17, 41), and again this is consistent with the enrichment of β-actin in the purified RNA granule fraction.

One alternative possibility for the structures that we isolated is aggregates of translating polyribosomes. Many of the RNA-binding proteins that we identified are also seen when proteomes of translating ribosomes are examined, including many of the hnRNPs, DEAD box proteins, and abundant RNA-binding proteins such as IEB2, -3, and G3BPs (31, 46, 47). One of the models for RNA transport is that RNAs are transported as aggregates of stalled polyribosomes that can be broken up into translating polyribosomes by activity. Thus, it would be difficult to distinguish between these two structures by proteomics. However, one argument against the presence of translating polyribosomes is the isolation of the ribosome aggregates only from developing brain and not from adult brain or other tissues. Because the purification conditions were identical to those used in E18 preparations, aggregated polyribosomes should also have been isolated from these preparations as well if aggregation of polysomes was simply an artifact of the purification strategy. In addition, one of the proteins identified in our proteome, RNA granule protein 105, has been proposed to separate from the RNA granule during the activation of the granule for translation (45), consistent with the assumption that we purified RNA granules and not polysomes. The enrichment for transported mRNAs but not general RNAs also argues strongly for a transport structure instead of simply aggregated polysomes.

Multiple Types of mRNA Granules—The lack of complete co-localization for the proteins and/or markers we tested suggests that there may be multiple types of mRNA granules. For

Downloaded from https://www.mcponline.org by guest on October 20, 2020

example, DEAD box 3 and CGI-99 mainly localized to distinct puncta. Moreover neither of those two markers was highly co-localized with Staufen 2, another marker used for RNA granules. It is not clear at this point whether there are indeed distinct types of granules, whether granules by their nature are heterogeneous depending on the specific mRNAs that they contain, whether the composition of these granules is dynamic, or whether these differences simply reflect technical issues in our localization studies.

DEAD box 3 is an RNA helicase that has been implicated in both nuclear export and translation initiation (48–50). DEAD box 3-containing puncta contain both the small and large ribosomal subunits as well as poly(A) RNA and thus can be clearly designated as RNA granules. The movement of DEAD box 3 in dendrites confirm this possibility. Although both ribosomal subunits may be independently stored in the granules and only reassembled once localized, it is likely that they are transported in the granules as 80 S ribosomes or polysomes. Therefore, how is the translation of their associated mRNA repressed? Regulation of translation in these granules is presumably at the stage of elongation either by preventing initiation of elongation or by halting a translating step. The identification in the proteomics of the T-complex polypeptide-1 chaperone complex and nascent polypeptide-associated complex-α (Supplemental Table S1) that are implicated in the stabilization of nascent proteins (51) is consistent with the latter hypothesis. There are a number of examples where mRNAs appear to be blocked in elongation at the polysome stage (52–54), and possible mechanisms could be through micro-RNAs, interaction between 5′- and 3′-binding proteins, or mechanisms similar to those involved in translocating mRNA/ribosomes to the ER. Indeed the correct repression of Oskar mRNA in *Drosophila* oogenesis depends on proteins important for stabilization of nascent chains (52). Interestingly many of these proteins that we identified (*e.g.* G3BP1, ELAVs, PA1–1, polypyrimidine tract-binding protein, and others) are also associated with polyribosomes isolated from brains (31, 46), consistent with a model where transport at this stage is in the form of stalled polyribosomes.

Conclusion—We generated a biochemical fraction from developing brain enriched for an RNA granule. The abundant components of this fraction were identified suggesting a structure made up of ribosomes, RNA-binding proteins, and RNAs attached to the cytoskeleton. We would suggest that the granules we isolated, enriched in β-actin mRNA, are involved in growth, whereas the KIF5a granule is involved in constitutive transport of dendritic mRNAs such as CaMKIIα. Elucidating how these distinct granules are regulated and transported will allow for a detailed understanding of the specificity and regulation of RNA transport in neurons.

* This work was supported in part by a Canadian Institutes of Health Research (CIHR) Group Grant MGC-57079 (to L. D. G., J.-C. L., and W. S. S.), CIHR Grants MT-15121 (to W. S. S.) and MOP-62751 (to L. D. G.), and operating grants from the Genome Quebec project: Réseau Protéomique de Montréal, Montreal Proteomics Network (RPMPN). The costs of publication of this article were defrayed in part by the payment of page charges. This article must therefore be hereby marked "*advertisement*" in accordance with 18 U.S.C. Section 1734 solely to indicate this fact.

S The on-line version of this article (available at http://www.mcponline.org) contains supplemental material.

¶ Supported by a CIHR studentship.

§§ Recipient of the Canada Research Chair in Cellular and Molecular Neurophysiology.

¶¶ Supported by a CIHR Investigator award and a William Dawson scholar.

‖‖ Supported by a CIHR Investigator award and a William Dawson scholar. To whom correspondence should be addressed: Dept. of Neurology and Neurosurgery, McGill University Montreal Neurological Inst., BT 110 3801 rue University, Montreal, Quebec H3A 2B4, Canada. Tel.: 514-398-1486; Fax:. 514-398-8106; E-mail: wayne.sossin@mcgill.ca.

REFERENCES

1. Gingras, A. C., Raught, B., and Sonenberg, N. (1999) eIF4 initiation factors: effectors of mRNA recruitment to ribosomes and regulators of translation. *Annu. Rev. Biochem.* **68,** 913–963
2. Walter, P., and Johnson, A. E. (1994) Signal sequence recognition and protein targeting to the endoplasmic reticulum membrane. *Annu. Rev. Cell Biol.* **10,** 87–119
3. Jansen, R. P. (2001) mRNA localization: message on the move. *Nat. Rev. Mol. Cell Biol.* **2,** 247–256
4. Kiebler, M. A., and DesGroseillers, L. (2000) Molecular insights into mRNA transport and local translation in the mammalian nervous system. *Neuron* **25,** 19–28
5. Bassell, G. J., Oleynikov, Y., and Singer, R. H. (1999) The travels of mRNAs through all cells large and small. *FASEB J.* **13,** 447–454
6. Lasko, P. (1999) RNA sorting in Drosophila oocytes and embryos. *FASEB J.* **13,** 421–433
7. Schuman, E. M. (1999) mRNA trafficking and local protein synthesis at the synapse. *Neuron* **23,** 645–648
8. Steward, O., Wallace, C. S., Lyford, G. L., and Worley, P. F. (1998) Synaptic activation causes the mRNA for the IEG Arc to localize selectively near activated postsynaptic sites on dendrites. *Neuron* **21,** 741–751
9. Brittis, P. A., Lu, Q., and Flanagan, J. G. (2002) Axonal protein synthesis provides a mechanism for localized regulation at an intermediate target. *Cell* **110,** 223–235
10. Crino, P. B., and Eberwine, J. (1996) Molecular characterization of the dendritic growth cone: regulated mRNA transport and local protein synthesis. *Neuron* **17,** 1173–1187
11. Bassell, G. J., Zhang, H., Byrd, A. L., Femino, A. M., Singer, R. H., Taneja, K. L., Lifshitz, L. M., Herman, I. M., and Kosik, K. S. (1998) Sorting of β-actin mRNA and protein to neurites and growth cones in culture. *J. Neurosci.* **18,** 251–265
12. Knowles, R. B., Sabry, J. H., Martone, M. E., Deerinck, T. J., Ellisman, M. H., Bassell, G. J., and Kosik, K. S. (1996) Translocation of RNA granules in living neurons. *J. Neurosci.* **16,** 7812–7820
13. Kohrmann, M., Luo, M., Kaether, C., DesGroseillers, L., Dotti, C. G., and Kiebler, M. A. (1999) Microtubule-dependent recruitment of Staufen-green fluorescent protein into large RNA-containing granules and subsequent dendritic transport in living hippocampal neurons. *Mol. Biol. Cell* **10,** 2945–2953
14. Krichevsky, A. M., and Kosik, K. S. (2001) Neuronal RNA granules: a link between RNA localization and stimulation-dependent translation. *Neuron* **32,** 683–696
15. Tang, S. J., Meulemans, D., Vazquez, L., Colaco, N., and Schuman, E. (2001) A role for a rat homolog of staufen in the transport of RNA to neuronal dendrites. *Neuron* **32,** 463–475
16. Kanai, Y., Dohmae, N., and Hirokawa, N. (2004) Kinesin transports RNA: isolation and characterization of an RNA-transporting granule. *Neuron* **43,** 513–525

Downloaded from https://www.mcponline.org by guest on October 20, 2020

17. Zhang, H. L., Singer, R. H., and Bassell, G. J. (1999) Neurotrophin regulation of β-actin mRNA and protein localization within growth cones. *J. Cell Biol.* **147,** 59–70
18. Gu, W., Pan, F., Zhang, H., Bassell, G. J., and Singer, R. H. (2002) A predominantly nuclear protein affecting cytoplasmic localization of β-actin mRNA in fibroblasts and neurons. *J. Cell Biol.* **156,** 41–51
19. Tiruchinapalli, D. M., Oleynikov, Y., Kelic, S., Shenoy, S. M., Hartley, A., Stanton, P. K., Singer, R. H., and Bassell, G. J. (2003) Activity-dependent trafficking and dynamic localization of zipcode binding protein 1 and β-actin mRNA in dendrites and spines of hippocampal neurons. *J. Neurosci.* **23,** 3251–3261
20. Shan, J., Munro, T. P., Barbarese, E., Carson, J. H., and Smith, R. (2003) A molecular mechanism for mRNA trafficking in neuronal dendrites. *J. Neurosci.* **23,** 8859–8866
21. Maycox, P. R., Link, E., Reetz, A., Morris, S. A., and Jahn, R. (1992) Clathrin-coated vesicles in nervous tissue are involved primarily in synaptic vesicle recycling. *J. Cell Biol.* **118,** 1379–1388
22. Wasiak, S., Legendre-Guillemin, V., Puertollano, R., Blondeau, F., Girard, M., de Heuvel, E., Boismenu, D., Bell, A. W., Bonifacino, J. S., and McPherson, P. S. (2002) Enthoprotin: a novel clathrin-associated protein identified through subcellular proteomics. *J. Cell Biol.* **158,** 855–862
23. Blondeau, F., Ritter, B., Allaire, P. D., Wasiak, S., Girard, M., Hussain, N. K., Angers, A., Legendre-Guillemin, V., Roy, L., Boismenu, D., Kearney, R. E., Bell, A. W., M., Bergeron, J. J., and McPherson, P. S. (2004). Tandem mass spectrometry analysis of brain clathrin-coated vesicles reveals their critical involvement in synaptic vesicle recycling. *Proc. Natl. Acad. Sci. U. S. A.* **101,** 3833–3838
24. Banker, G., and Goslin, K. (1988) Developments in neuronal cell culture. *Nature* **336,** 185–186
25. Duchaine, T. F., Hemraj, I., Furic, L., Deitinghoff, A., Kiebler, M. A., and DesGroseillers, L. (2002) Staufen2 isoforms localize to the somatodendritic domain of neurons and interact with different organelles. *J. Cell Sci.* **115,** 3285–3295
26. Kelm, R. J., Jr., Cogan, J. G., Elder, P. K., Strauch, A. R., and Getz, M. J. (1999) Molecular interactions between single-stranded DNA-binding proteins associated with an essential MCAT element in the mouse smooth muscle α-actin promoter. *J. Biol. Chem.* **274,** 14238–14245
27. Aschrafi, A., Cunningham, B. A., Edelman, G. M., and Vanderklish, P. W. (2005) The fragile X mental retardation protein and group I metabotropic glutamate receptors regulate levels of mRNA granules in brain. *Proc. Natl. Acad. Sci. U. S. A.* **102,** 2180–2185
28. Ohashi, S., Kobayashi, S., Omori, A., Ohara, S., Omae, A., Muramatsu, T., Li, Y., and Anzai, K. (2000) The single-stranded DNA- and RNA-binding proteins purα and purβ link BC1 RNA to microtubules through binding to the dendrite-targeting RNA motifs. *J. Neurochem.* **75,** 1781–1790
29. De Diego Otero, Y., Severijnen, L. A., van Cappellen, G., Schrier, M., Oostra, B., and Willemsen, R. (2002) Transport of fragile X mental retardation protein via granules in neurites of PC12 cells. *Mol. Cell Biol.* **22,** 8332–8341
30. Schenck, A., Bardoni, B., Moro, A., Bagni, C., and Mandel, J. L. (2001) A highly conserved protein family interacting with the fragile X mental retardation protein (FMRP) and displaying selective interactions with FMRP-related proteins FXR1P and FXR2P. *Proc. Natl. Acad. Sci. U. S. A.* **98,** 8844–8849
31. Angenstein, F., Evans, A. M., Settlage, R. E., Moran, S. T., Ling, S. C., Klintsova, A. Y., Shabanowitz, J., Hunt, D. F., and Greenough, W. T. (2002) A receptor for activated C kinase is part of messenger ribonucleoprotein complexes associated with polyA-mRNAs in neurons. *J. Neurosci.* **22,** 8827–8837
32. Shor, B., Calaycay, J., Rushbrook, J., and McLeod, M. (2003) Cpc2/RACK1 Is a ribosome-associated protein that promotes efficient translation in *Schizosaccharomyces pombe*. *J. Biol. Chem.* **278,** 49119–49128
33. Ceci, M., Gaviraghi, C., Gorrini, C., Sala, L. A., Offenhauser, N., Marchisio, P. C., and Biffo, S. (2003) Release of eIF6 (p27BBP) from the 60S subunit allows 80S ribosome assembly. *Nature* **426,** 579–584
34. Wilkie, G. S., and Davis, I. (2001) Drosophila wingless and pair-rule transcripts localize apically by dynein-mediated transport of RNA particles. *Cell* **105,** 209–219
35. Tekotte, H., and Davis, I. (2002) Intracellular mRNA localization: motors move messages. *Trends Genet.* **18,** 636–642
36. Huang, Y. S., Carson, J. H., Barbarese, E., and Richter, J. D. (2003) Facilitation of dendritic mRNA transport by CPEB. *Genes Dev.* **17,** 638–653
37. Bannai, H., Fukatsu, K., Mizutani, A., Natsume, T., Iemura, S., Ikegami, T., Inoue, T., and Mikoshiba, K. (2004) An RNA-interacting protein, SYNCRIP (heterogeneous nuclear ribonuclear protein Q1/NSAP1) is a component of mRNA granule transported with inositol 1,4,5-trisphosphate receptor type 1 mRNA in neuronal dendrites. *J. Biol. Chem.* **279,** 53427–53434
38. Zhang, H. L., Eom, T., Oleynikov, Y., Shenoy, S. M., Liebelt, D. A., Dictenberg, J. B., Singer, R. H., and Bassell, G. J. (2001) Neurotrophin-induced transport of a β-actin mRNP complex increases β-actin levels and stimulates growth cone motility. *Neuron* **31,** 261–275
39. Rook, M. S., Lu, M., and Kosik, K. S. (2000) CaMKIIα 3′ untranslated region-directed mRNA translocation in living neurons: visualization by GFP linkage. *J. Neurosci.* **20,** 6385–6393
40. Knowles, R. B., and Kosik, K. S. (1997) Neurotrophin-3 signals redistribute RNA in neurons. *Proc. Natl. Acad. Sci. U. S. A.* **94,** 14804–14808
41. Willis, D., Li, K. W., Zheng, J.-Q., Chang, J. H., Smit, A., Kelly, T., Merianda, T. T., Sylvester, J., van Minnen, J., and Twiss, J. L. (2005) Differential transport and local translation of cytoskeletal, injury-response, and neurodegeneration protein mRNAs in axons. *J. Neurosci.* **25,** 778–791
42. Brunet, S., Thibault, P., Gagnon, E., Kearney, P., Bergeron, J. J., and Desjardins, M. (2003) Organelle proteomics: looking at less to see more. *Trends Cell Biol.* **13,** 629–638
43. Ritter, B., Blondeau, F., Denisov, A. Y., Gehring, K., and McPherson, P. S. (2004) Molecular mechanisms in clathrin-mediated membrane budding revealed through subcellular proteomics. *Biochem. Soc. Trans.* **32,** 769–773
44. Huarte, M., Sanz-Ezquerro, J. J., Roncal, F., Ortin, J., and Nieto, A. (2001) PA subunit from influenza virus polymerase complex interacts with a cellular protein with homology to a family of transcriptional activators. *J. Virol.* **75,** 8597–8604
45. Shiina, N., Shinkura, K., and Tokunaga, M. (2005) A novel RNA-binding protein in neuronal RNA granules: regulatory machinery for local translation. *J. Neurosci.* **25,** 4420–4434
46. Khandjian, E. W., Huot, M. E., Tremblay, S., Davidovic, L., Mazroui, R., and Bardoni, B. (2004) Biochemical evidence for the association of fragile X mental retardation protein with brain polyribosomal ribonucleoparticles. *Proc. Natl. Acad. Sci. U. S. A.* **101,** 13357–13362
47. Angenstein, F., Evans, A. M., Ling, S. C., Settlage, R. E., Ficarro, S., Carrero-Martinez, F. A., Shabanowitz, J., Hunt, D. F., and Greenough, W. T. (2005) Proteomic characterization of messenger ribonucleoprotein complexes bound to nontranslated or translated poly(A) mRNAs in the rat cerebral cortex. *J. Biol. Chem.* **280,** 6496–6503
48. Chuang, R. Y., Weaver, P. L., Liu, Z., and Chang, T. H. (1997) Requirement of the DEAD-Box protein ded1p for messenger RNA translation. *Science* **275,** 1468–1471
49. Askjaer, P., Rosendahl, R., and Kjems, J. (2000) Nuclear export of the DEAD box An3 protein by CRM1 is coupled to An3 helicase activity. *J. Biol. Chem.* **275,** 11561–11568
50. Yedavalli, V. S., Neuveut, C., Chi, Y. H., Kleiman, L., and Jeang, K. T. (2004) Requirement of DDX3 DEAD box RNA helicase for HIV-1 Rev-RRE export function. *Cell* **119,** 381–392
51. McCallum, C. D., Do, H., Johnson, A. E., and Frydman, J. (2000) The interaction of the chaperonin tailless complex polypeptide 1 (TCP1) ring complex (TRiC) with ribosome-bound nascent chains examined using photo-cross-linking. *J. Cell Biol.* **149,** 591–602
52. Braat, A. K., Yan, N., Arn, E., Harrison, D., and Macdonald, P. M. (2004) Localization-dependent oskar protein accumulation; control after the initiation of translation. *Dev. Cell* **7,** 125–131
53. Ruegsegger, U., Leber, J. H., and Walter, P. (2001) Block of HAC1 mRNA translation by long-range base pairing is released by cytoplasmic splicing upon induction of the unfolded protein response. *Cell* **107,** 103–114
54. Clark, I. E., Wyckoff, D., and Gavis, E. R. (2000) Synthesis of the posterior determinant Nanos is spatially restricted by a novel cotranslational regulatory mechanism. *Curr. Biol.* **10,** 1311–1314
55. Mizutani, A., Fukuda, M., Ibata, K., Shiraishi, Y., and Mikoshiba, K. (2000) SYNCRIP, a cytoplasmic counterpart of heterogeneous nuclear ribonucleoprotein R, interacts with ubiquitous synaptotagmin isoforms. *J. Biol. Chem.* **275,** 9823–9831
56. Lau, P. P., Chang, B. H., and Chan, L. (2001) Two-hybrid cloning identifies

Downloaded from https://www.mcponline.org by guest on October 20, 2020

an RNA-binding protein, GRY-RBP, as a component of apobec-1 editosome. *Biochem. Biophys. Res. Commun.* **282,** 977–983
57. Gallouzi, I. E., Parker, F., Chebli, K., Maurier, F., Labourier, E., Barlat, I., Capony, J. P., Tocque, B., and Tazi, J. (1998) A novel phosphorylation-dependent RNase activity of GAP-SH3 binding protein: a potential link between signal transduction and RNA stability. *Mol. Cell. Biol.* **18,** 3956–3965
58. Good, P. J. (1995) A conserved family of elav-like genes in vertebrates. *Proc. Natl. Acad. Sci. U. S. A.* **92,** 4557–4561
59. Good, P. J. (1997) The role of elav-like genes, a conserved family encoding RNA-binding proteins, in growth and development. *Semin. Cell Dev. Biol.* **8,** 577–584
60. Kao, P. N., Chen, L., Brock, G., Ng, J., Kenny, J., Smith, A. J., and Corthesy, B. (1994) Cloning and expression of cyclosporin A- and FK506-sensitive nuclear factor of activated T-cells: NF45 and NF90. *J. Biol. Chem.* **269,** 20691–20699
61. Langland, J. O., Kao, P. N., and Jacobs, B. L. (1999) Nuclear factor-90 of activated T-cells: a double-stranded RNA-binding protein and substrate for the double-stranded RNA-dependent protein kinase, PKR. *Biochemistry* **38,** 6361–6368
62. Nakagawa, T. Y., Swanson, M. S., Wold, B. J., and Dreyfuss, G. (1986) Molecular cloning of cDNA for the nuclear ribonucleoprotein particle C proteins: a conserved gene family. *Proc. Natl. Acad. Sci. U. S. A.* **83,** 2007–2011

Downloaded from https://www.mcponline.org by guest on October 20, 2020